
SURFACES, INTERFACES,
AND THIN FILMS

Comparative Study on Structural, Optical, and Electrical Properties of ZnO Thin Films Prepared by PLD and Sputtering Techniques

H. Naeem-ur-Rehman Khan^{a,b}, M. Mehmood^{a,*}, F. C. C. Ling^b, A. Faheem Khan^{c,d,e}, and S. M. Ali^f

^a Department of Physics, Khwaja Fareed University of Engineering and Information Technology, Rahim Yar Khan, 64200 Pakistan

^b Department of Metallurgy and Materials Engineering, Pakistan Institute of Engineering and Applied Sciences, Islamabad, 45650 Pakistan

^c Department of Physics, The University of Hong Kong, Pokfulam Road, Hong Kong, China

^d Department of Materials Science and Engineering, Institute of Space Sciences, Islamabad, Pakistan

^e UM Power Energy Dedicated Advanced Centre (UMPEDAC), Level 4, Wisma R&D UM, University of Malaya, Jalan Pantai Baharu, Kuala Lumpur, 59990 Malaysia

^f Department of Physics and Astronomy, King Saud University, Riyadh, Saudi Arabia

*e-mail: mazhar@pieas.edu.pk

Received August 22, 2017; revised May 14, 2020; accepted May 21, 2020

Abstract—ZnO thin films were formed on *c*-plane sapphire and p-GaN substrates by pulsed laser deposition (PLD) and radio frequency (RF) magnetron sputtering techniques. XRD analysis including omega scan depicted the formation of highly textured wurtzite ZnO with *c*-axis. The texture was primarily introduced by the substrate effects as the planes lying at oblique angles also exhibited six-fold symmetry during phi scan. Atomic force microscopy exhibited the surface roughness of 4.33 and 12.99 nm for PLD and sputtered ZnO films, respectively. In photoluminescence (PL) measurements, a strong UV emission was observed at 3.30 eV for both ZnO films. However, deep-level emission was observed at around 2.61 eV in PLD film, but it had a wide range from 2.61 to 2.29 eV in case of sputter-deposited film. From the transmission spectra, the optical band gap values were found to be 3.29 and 3.28 eV for PLD and sputtered ZnO films, respectively. Hall measurement revealed the resistivity values of 0.0792 and 0.4832 Ω cm and carrier concentrations of 2.28×10^{18} and 1.73×10^{18} cm⁻³ for respective PLD and sputtered films. *I(V)* current–voltage curves clearly demonstrated the n-ZnO/p-GaN hetero-junction with turn-on voltage of 3.8 and 5.2 V for PLD and sputtered samples, respectively.

Keywords: zinc oxide, RF magnetron sputtering, pulsed laser deposition, photoluminescence, hetero-junction

DOI: 10.1134/S1063782620090201

1. INTRODUCTION

Zinc oxide (ZnO) is one of the most widely used semiconducting materials due to its large and direct band gap (3.37 eV) making it suitable for a variety of electrical and optical device applications [1, 2]. Due to its large exciton binding energy (60 meV) at room temperature in comparison with GaN (26 meV), it can be employed for many potential applications in optoelectronic devices such as solar cells, gas sensors, lasers, wave devices, luminescent materials, etc. [3]. The larger exciton binding energy of ZnO makes it a promising material for exciton emission at room temperature under low binding energy. That's why, it has potential use for short-wavelength optoelectronic devices. The increased usage of short-wavelength optoelectronics devices in industry has forced the researchers to explore the structural, optical, electri-

cal, and optoelectronic properties of ZnO at room temperature as well as at elevated temperatures. Henceforth, there is non-stop motivation to report synthesis and characterization of ZnO in the form of bulk material as well as thin film. Zu et al. [4] investigated the optical emission properties of ZnO thin films prepared by MBE at room temperature for optoelectronic applications. They proved that optical properties of ZnO thin films is composed of two regions: one is the excitonic near the band edge due to the energy equal to the band gap of ZnO, and the other is deep-level emission due to defects in the visible range. Deep-level emission arises due to intrinsic defects such as oxygen vacancies, interstitial, zinc vacancies, extrinsic impurities, etc. [5]. Generally, UV emission is thought to be due to exciton transition [6]. Nevertheless, the precise origin of visible emission is still not well-understood and needs further research due to

multiple defects in the ZnO films such as intrinsic defects. Furthermore, it is well-established fact that the optical, electrical, and opto-electronic properties of ZnO films are sensitive to crystalline quality and smoothness of the films. Consequently, most of the work has been performed on controlling the defects and to improve the quality of ZnO thin film. It has been reported that the improvement in the crystal quality may cause the appearance of a sharp and strong UV emission and a suppressed and weak green emission [7–9].

Presently, most of the industrial applications employ the wide-band-gap semiconductors, especially GaN (a III–V group semiconductor) and its alloys. However, GaN-based light-emitting diodes (LEDs) generally have higher threshold and are unable to work at higher temperature because of its small excitonic binding energy of about 26 meV. On the other hand, owing to better properties of ZnO at elevated temperatures and higher excitonic binding energy, it is a good choice to replace GaN for working in harsh environment and at high temperatures [10, 11].

As an intrinsic *n*-type material, ZnO needs a *p*-type semiconductor material to make a *p*–*n* junction for an LED. Stable and reproducible *p*-type conductivity for ZnO is still a very difficult task. Some groups have reported the deposition of *p*-ZnO and used it for making homo-junction with *n*-ZnO to get an LED [12–15]. But still there is a question mark on the stability and reproducibility of this ZnO homo-junction. Based on above-mentioned limitations, many researchers have used GaN [16–19], Si [20–22], and NiO [23–25] as a *p*-type material for combination with ZnO to have a successful *p*–*n* junction diode. Unlike other *p*-type materials, GaN has the wurtzite crystal structure resembling that of ZnO with comparatively very low lattice mismatch $\sim 1.8\%$ [26] and a comparable band gap. Moreover, GaN is technically more stable for longer duration than all its counterparts.

ZnO films have been deposited by various techniques such as evaporation [27], molecular beam epitaxy [28], pulsed laser deposition (PLD) [17], sputtering, metal organic chemical vapor deposition [9, 18], electrodeposition [29], etc. Nevertheless, PLD has advantages such as oriented growth of films (at low substrate temperature), high deposition rates, deposition at high oxygen pressure, and good quality of films. Whereas, sputtering offers good adhesion, high deposition rate, high degree of crystallinity with (002) peak (and rocking curve having less FWHM), high optical transmittance, and sputtering of almost any compound. Radio-frequency (RF) magnetron sputtering [18, 30] and PLD [26] have been employed by different groups to make hetero-junction of *n*-ZnO on *p*-GaN substrate. In the present work, ZnO films have been deposited on the *p*-GaN substrate using RF magnetron sputtering and PLD and tried to compare

their morphology and investigate and correlate the structural, optical, and electrical characteristics of ZnO film deposited by different techniques and the hetero-junction with *p*-GaN. Growth patterns of ZnO hetero-structures on GaN were probed for respective deposited films in order to understand the basic phenomenon behind various optical and electrical properties. ZnO|GaN hetero-junction grown by PLD has been found to be better in efficiency (in terms of higher current and lower threshold voltage) in comparison with RF magnetron sputtering owing to its inherent controlled growth conditions.

2. EXPERIMENTAL PROCEDURE

The ZnO target for the sputter deposition was prepared using ZnO powder with 99.99% purity. The ZnO powder was pulverized thoroughly for two hours, and then a pellet of 50-mm diameter and 3-mm thickness was prepared with subsequent sintering at 1200°C for 12 h. Two types of substrates were used in this study. For structural properties, ZnO films were deposited on the *c*-plane sapphire substrate, while the current–voltage study of the *p*-GaN|*n*-ZnO hetero-junction were studied by depositing ZnO films on the commercially available *p*-Mg:GaN (carrier concentration $\sim 5 \times 10^{18} \text{ cm}^{-3}$) deposited on *c*-plane sapphire. The substrates were cleaned subsequently with acetone, ethanol, and deionized water each for 10 min before deposition. PLD and RF magnetron sputtering techniques were employed in this experiment. The first sample was prepared by using PLD system (with Coherent COMPexPro 102 KrF laser, 248-nm wavelength, max pulse energy = 400 mJ). The chamber was evacuated to a base pressure of 6×10^{-4} Pa before deposition with substrate temperature at 600°C, and target to substrate distance was maintained at 8 cm. A laser beam of 300 mJ with a frequency of 2 Hz was used to ablate ZnO target. The oxygen partial pressure during the deposition was kept at 2 Pa and depositing time was 60 min. Film thickness (~ 180 nm) was measured by field emission scanning electron microscopy (FESEM). The second sample was deposited by the RF magnetron sputtering system using the same ZnO target. The deposition chamber was evacuated to a base pressure of 5.5×10^{-4} Pa before deposition. Substrates were placed at the substrate holder 8 cm away from the ZnO target and the deposition temperature for the ZnO was kept at 600°C. The argon gas (99.999% pure) was introduced into the chamber as sputtering medium. The pre-sputtering was performed for about 10 min to clean the surface of the target. The working pressure during the deposition was kept at 1 Pa and the deposition time for ZnO film was 6 hours. The thickness of the film was estimated to be ~ 860 nm during deposition.

The crystal structure of both samples was analyzed using Bruker D8 Advance X-ray diffractometer

equipped with $\text{CuK}\alpha$ line (0.1541 nm). Surface morphology of the films was investigated by atomic force microscopy (Quesant Universal SPM, Ambios Technology, USA) in non-contact mode. Room-temperature photoluminescence (PL) measurements were performed with 325-nm He–Cd laser line (Melles Griot Series 56) at 15 mW. Room-temperature electrical properties were determined using Hall Effect measurement with van der Pauw configuration by the Accent HL-5500PC system. Optical transmittance spectra of the ZnO films were obtained at room temperature using Mapada UV-3200PC Spectrophotometer in the wavelength range of 200 to 800 nm. The current–voltage measurements for the ZnO/GaN hetero-structures were obtained by using hp 4155A Semiconductor parameter analyzer in the voltage range of 10 to -10 V.

3. RESULTS AND DISCUSSION

Figure 1a represents XRD patterns for the ZnO thin films deposited on *c*-plane sapphire substrates.

Both the PLD-grown and sputtered samples exhibit a preferred (002)-oriented growth along *c*-axis. Similar results have been obtained by Lee et al. and Kumar et al. [31, 32] for ZnO films prepared by PLD. To further investigate the film quality and crystallographic orientation, rocking curves for the (002) peak were obtained as shown in Fig. 1b. These curves reveal the variation in the degree of texture in both samples. The full width at half maximum (FWHM) of peaks was calculated to be 1.87° and 4.75° for the PLD- and sputter-formed ZnO films, respectively. The FWHM for the PLD sample is much narrower, which may be related to higher crystalline quality or improved orientation relationship with the substrate in comparison with the sputtered film. Zhao-yang et al. [33] have reported that the quality of the films improves with the increase in substrate temperature due to higher thermal energy/diffusivity of the adatoms. In our case, substrate temperature is same for both the films. Nevertheless, PLD technique is characterized by extremely high energy of the vaporized atoms in the plume. The energetic flux of incident atoms seems to provide additional energy to the atoms at the surface for higher crystalline quality of the film with excellent growth along *c*-axis. The tendency of high energy incident particles to relieve the internal stresses of the film, thereby improving the crystallinity is also in agreement with Aravind et al. [34]. Anyway, it may be noted that even the sputtered film exhibits FWHM of only about 4° in the rocking curves, which is attributable to high substrate temperature as well as still a reasonable energy of the incident particles (known to be better than simple evaporation).

The highly oriented growth may also partly be due to the choice of single-crystal sapphire substrate and some degree of epitaxial growth. Phi scan of the ZnO (104) peak was employed to have some insight of in-

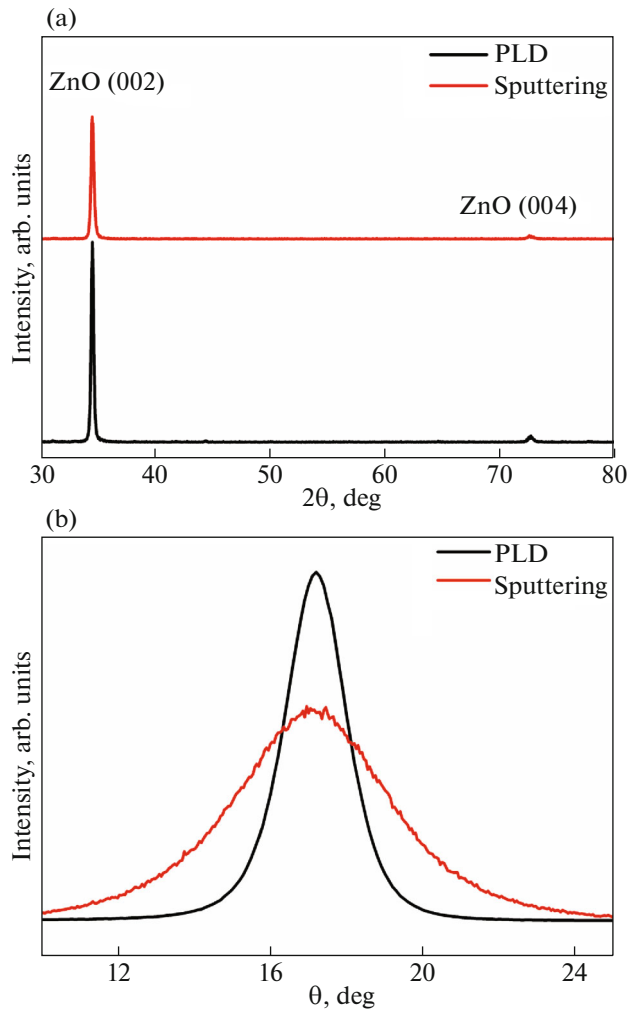


Fig. 1. (a) XRD spectra of PLD-grown and RF sputtered samples on sapphire substrate. (b) Rocking curve of the ZnO (002) peak for ZnO thin films.

plane orientation of both ZnO thin films in comparison with sapphire substrate (Fig. 2).

This peak was approached by suitably aligning the substrate with respect to diffraction geometry. As can be seen, both the samples exhibit six distinct peaks separated by 60° related with six-fold symmetry that clearly manifests the tendency of wurtzite ZnO to undergo epitaxial growth on single-crystal *c*-plane sapphire. The sharp peaks with a FWHM of 6° – 8° for the PLD-grown sample depicts a picture of good epitaxial growth as compared to the RF-sputtered sample, in which the peaks are much broader and of low peak-to-background ratio. Kim et al. [35] reported the relatively high temperature PLD-grown ZnO films yielded an improvement for in-plane and out-of-plane crystallinity.

Figure 3 depicts the typical top view AFM images of the PLD-grown and RF sputtered samples.

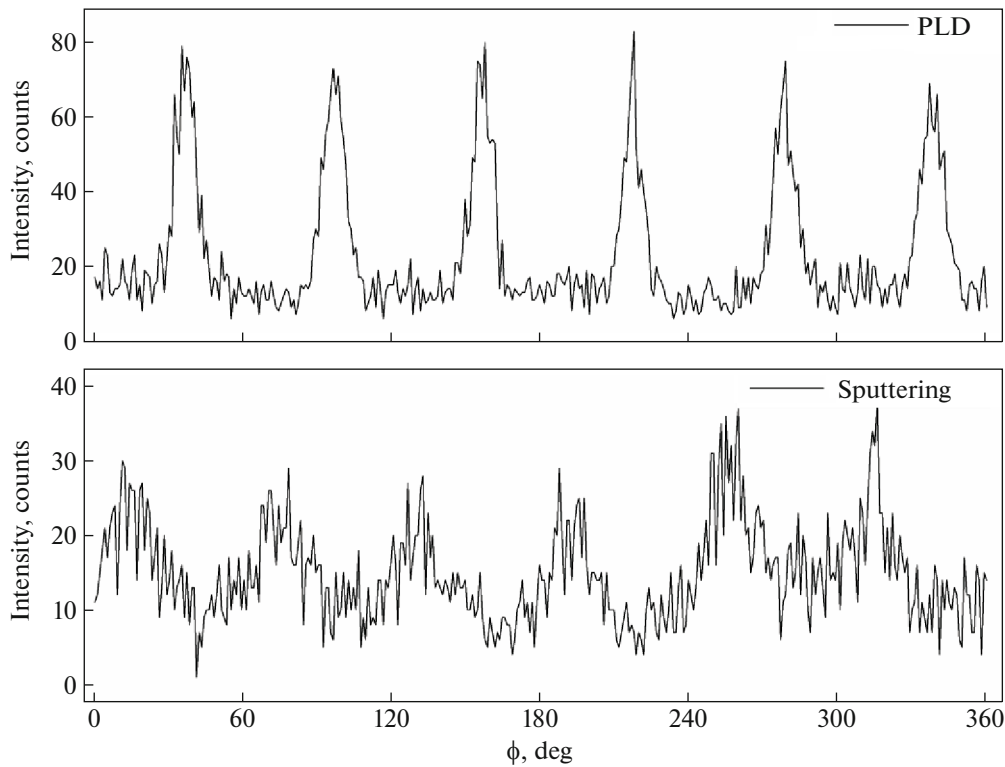


Fig. 2. X-ray phi scan of ZnO (104) reflection for PLD-grown and RF sputtered samples.

The bar assists to present z-height variation in the sample's surface. It may be noted that z-height variation in case of PLD film is of the order of 15 nm, much smaller than about 50 nm in sputtered film. On X - Y plane also the PLD film exhibits finer structure. The RMS roughness of PLD film is about 4.3 nm, which is much smaller than that for sputtered film, i.e., 12.9 nm. The surface roughness increases for sputtered films as compared to PLD-grown films showing non-uniform distribution of grain sizes clear from Fig. 3.

Figures 4a and 4b compare the top view SEM images of the films, while Figs. 4c and 4d present the cross-sectional views.

The coarser structure of sputtered film in comparison with PLD films is in close agreement with AFM images (Figs. 4a and 4b). In both cases, columnar growth is evident from Figs. 4c and 4d. These columns may possibly be crystals and/or sub-crystals separated by large and small-angle grain boundaries. Furthermore, a relatively more compact nature of the film formed by PLD is clearly evident (Figs. 4c and 4d). Higher energy incident particles in PLD may be responsible for compact deposits.

It may be suggested that the films nucleate on the substrate in typically epitaxial manner. However, due to large lattice mismatch, perfect 2D growth does not take place. The growth stresses are relaxed by forming islands, which finally grow upward in the form of col-

umns. These columns have certain degree of orientation relationship with the substrate that gives rise to six-fold in-plane symmetry in phi-axis. This orientation relationship is much stronger in case of PLD films, as the FWHM of the peaks along phi-axis is much finer in comparison with sputtered film. High energy of incident particles seems responsible for annealing out the defects and forming compact deposits with solid and dense inter-column boundaries in case of PLD films. Accordingly, the crystals/columns formed during growth do not find sufficient space to relax, as a result of which the crystals continue their growth almost in the same axis without much rotational adjustment. As a result, PLD film exhibits very small FWHM of peak in omega scan for the surface planes of (002) as well as in phi scan for an oblique angle plane of (104).

Figure 5 illustrates photoluminescence spectra of ZnO films formed by PLD and sputtering.

UV emission peak centered at 3.30 eV corresponds to near-band edge emission related with the direct recombination of free excitons [36].

Both the films exhibit a blue emission peak centered at 2.61 eV, while the sputtered film shows an additional green emission peak at 2.29 eV. Photoluminescence of ZnO in the visible region is generally related to intrinsic defects such as oxygen vacancies, zinc vacancies, zinc interstitials, etc. [37]. However, green luminescence is mostly observed in case of

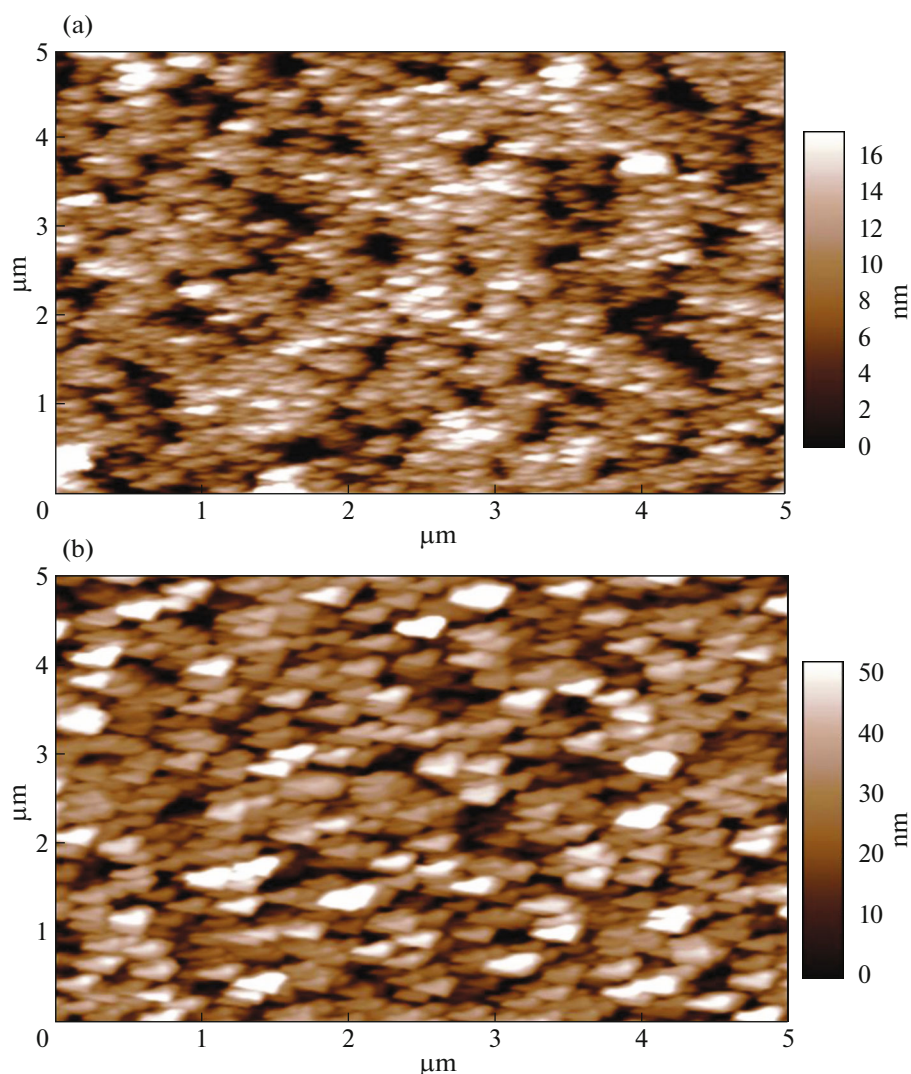


Fig. 3. AFM images: (a) PLD-grown, (b) RF-sputtered.

nanowires and nanorods, while blue luminescence is frequently observed in thin films. Son et al. [38] have observed shift from green luminescence for the films formed at lower temperatures to blue luminescence for the films formed at relatively higher temperatures with appearance of coarser columnar grains. Blue emission in spite of very high crystalline quality of the film formed by PLD suggests that this is not related to simply intrinsic intra-crystalline point defects; but it is related to defects in the inter-crystalline boundaries. For instance, the blue emission at 2.61 eV is attributable to the transition of charge carriers from zinc interstitial to ionized zinc vacancy level [39, 40]. This pair of defects may be situated at inter-columnar boundaries where crystals of high quality meet generating a boundary with variety of defects. Intensity of blue emission is increased in sputtered films despite a possible decrease in the overall column boundary regions due to larger size of columns. This seems related with

the fact that mutual mis-orientation of these columnar crystals along X - Y plane, where prismatic planes meet, is much less for the PLD films than for the sputtered film (Figs. 4c and 4d) as a result of which the former films have relatively lower number density of defects along the grain boundary. The green peak emission by sputtered ZnO sample might be related with common intrinsic point defects related with oxygen vacancies. One reason may be significant deficiency of oxygen/deviation from stoichiometry, as these films were formed in argon atmosphere; although lower crystalline perfection in sputtered film may be regarded as another reason for bluish-green emission by the sputtered films.

Figure 6 shows the room-temperature optical transmittance spectra of the PLD- and sputtering-formed ZnO thin films.

From the spectra of films, it is evident that the average transmittance value of around 90% lies in the

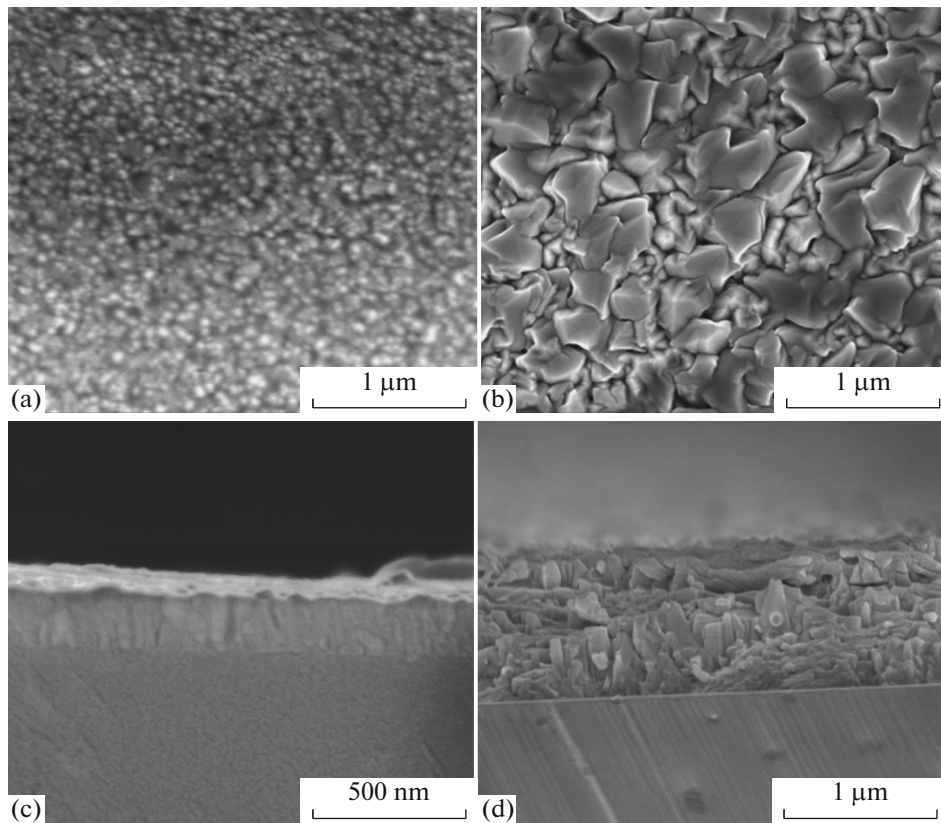


Fig. 4. Surface morphology of (a) PLD-grown, (b) RF-sputtered ZnO thin films; (c) and (d) represent the cross-sectional views of PLD-grown and sputtered films, respectively.

visible wavelength range, and absorption of at around 378 nm indicating high crystalline and optical quality, which indicates that the obtained films have low impurities and few lattice defects [41, 42]. The absorption edge corresponds to transition from valence band

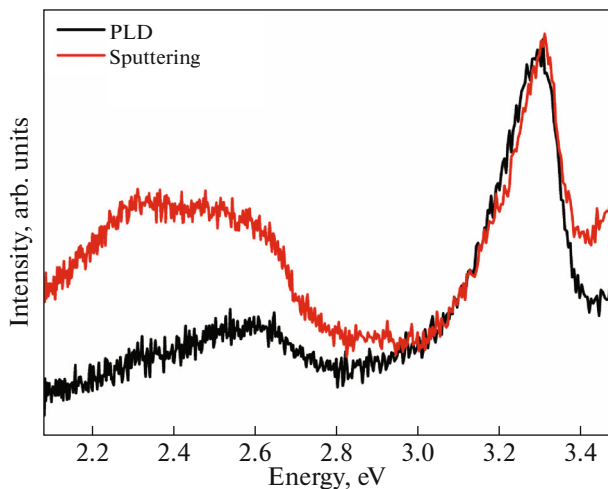


Fig. 5. Room-temperature PL spectra of ZnO thin films formed by PLD and RF sputtering.

to conduction band whereas; the absorption in the visible range is associated with intrinsic defects in the films [43]. The apparent steep drop off at 378 nm in the transmission line for PLD-grown ZnO films is shifted towards lower wavelength as compared to that of sputtered film also indicating that the optical gap in the film grown by PLD is larger than in film deposited by sputtering method. The band gap of both films can be estimated by calculating the absorption coefficient expressed by the relation [44]:

$$(\alpha h\nu) = A(h\nu - E_g)^{1/2}, \quad (1)$$

where A is a constant, α is the absorption coefficient, h is Planck's constant and ν is the frequency of incident radiation. E_g is determined by extrapolating the straight line portion of the spectrum to $\alpha h\nu = 0$. The observed direct band gap energy of the ZnO films deposited by sputtering and PLD are 3.28 and 3.29 eV, respectively. Interestingly, the band gap energy of the pure ZnO thin films increases with substrate temperatures [45]. In comparison to the band gap energy of single crystal ZnO (3.37 eV), these obtained values are somewhat smaller. This small variation of the band gap energy has been attributed to defects in ZnO thin films. These optical band gap values are in well matches with the reports on spray pyrolysis [46],

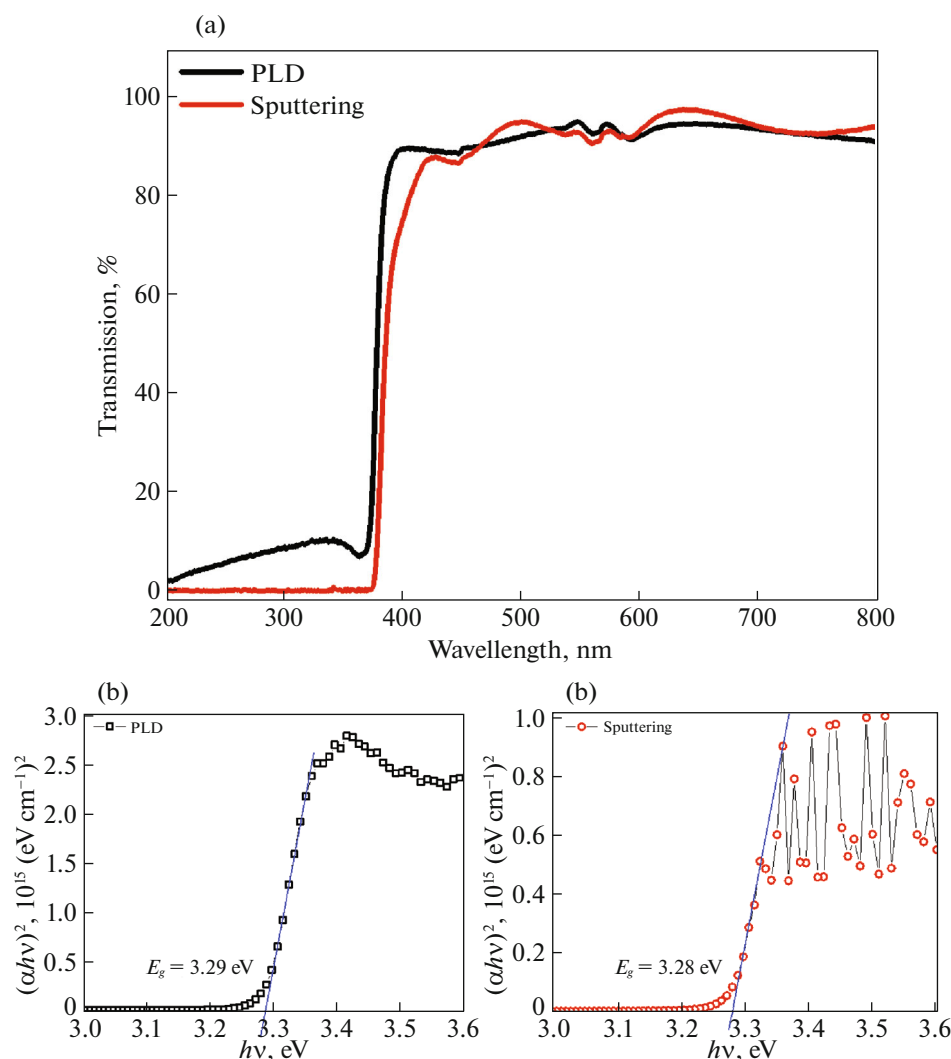


Fig. 6. (a) Transmission spectra of PLD-grown and RF-sputtered ZnO films; (b) shows the estimated band gap of the two samples.

RF sputtered [47], DC reactive magnetron sputtered [48], and ion beam sputtered [49] films. The higher band gap of PLD-grown ZnO films suggests that the PLD films have better crystalline quality than sputter deposited ZnO films.

The reflectance of ZnO thin films deposited by PLD and RF magnetron sputtering is shown in Fig. 7.

The reflectance behavior of both films is appeared to be different as PLD film is hitch-free while sputtering sample has shown an oscillatory fringe pattern in the measured range of wavelength. As seen, sputtered film exhibits a slightly low reflection as compared with PLD films in a wavelength range of 300–500 nm. The reduction of the reflection can be explained as for the transmittance in terms of free surface morphology. The intensity of diffusely transmitted light is controlled by the differences in the refractive index of ZnO and sapphire substrate, the ratio of light wave-

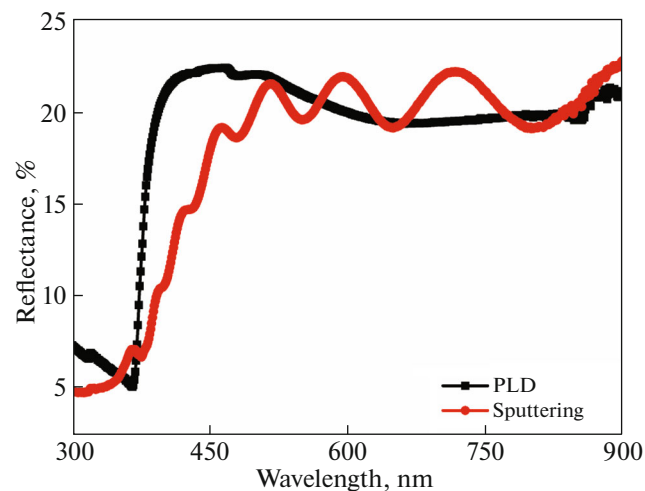


Fig. 7. Optical reflectance spectra of ZnO thin films formed by PLD and RF sputtering.

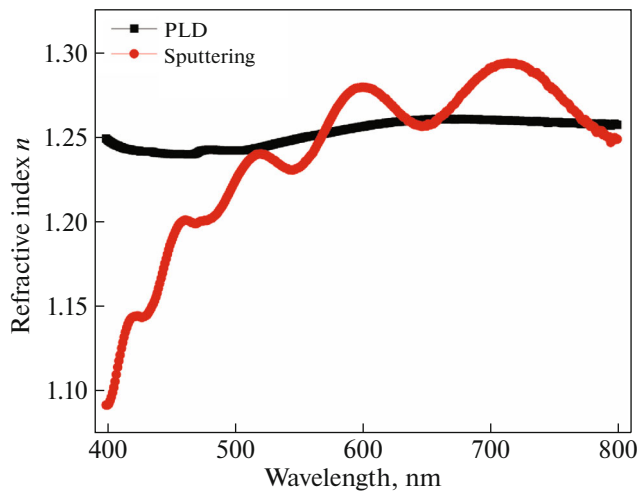


Fig. 8. Variation of refractive index n versus wavelength of ZnO thin films.

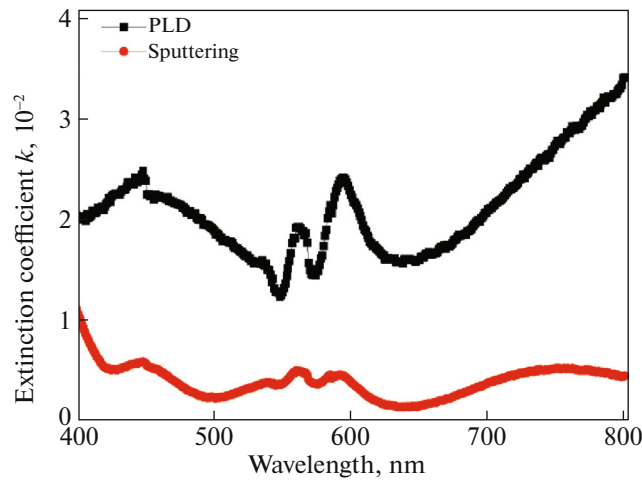


Fig. 9. Plot of extinction coefficient k versus wavelength for ZnO thin films.

length (λ) and the vertical RMS value (R) according to the scattering theory [50]. In the case of $R \ll \lambda$, the intensity of diffusely transmitted light is higher and with less amount of reflection losses. This theory shows a good agreement with our experimental results.

The refractive index of these films can be calculated from the reflectance data by the following relation [51]

$$n = \sqrt{\frac{1 + \sqrt{R}}{1 - \sqrt{R}}} \quad (2)$$

And the calculated refractive index has been plotted against wavelength in the visible region shown in Fig. 8.

It can be seen that refractive index of PLD-grown ZnO film exhibits almost same value around 1.25 for

the entire wavelength region. In contrast, the sputtered ZnO thin film has shown an oscillatory (from $n_{\min} = 1.09$ to $n_{\max} = 1.29$) behavior which tends to decrease with decreasing wavelength. These values of the refractive index are approximately close to the value reported for bulk material [52, 53].

The complex refractive index of thin films is defined as

$$n^* = n - ik, \quad (3)$$

where n^* is the complex refractive index and k is known as the imaginary part of n^* and is known as extinction coefficient. It can be calculated from the relation [54]

$$k = \frac{\alpha\lambda}{4\pi}. \quad (4)$$

And in this equation α is known as absorption coefficient and it can be calculated from the transmittance data using equation [55]

$$T = e^{-\alpha x}, \quad (5)$$

where T is transmittance and x denotes the thickness of the deposited film. By using these two equations, the extinction coefficient k has been calculated as a function of wavelength and plotted in Fig. 9.

The value of k is found to be consistent in the visible wavelength region with negligible variations for both samples. The steep rise (for sputtered ZnO films) in the value of the extinction coefficient near the band edge (<420 nm) is due to the inter-band absorption [56].

The relative permittivity ϵ of the PLD- and the sputtering-formed thin films has determined using the relation $\epsilon = n^2$ and is plotted as a function of wavelength as shown in Fig. 10.

The low frequency shows a larger dielectric constant, which is due to the presence of space charge polarization [57]. The decrease of dielectric constant with increasing frequency can be explained by the fact that the frequency of electric charge carriers cannot follow the alternation of the ac electric field applied beyond a certain critical frequency [58]. The higher frequencies show very small dielectric constant, which is key for the fabrication of materials for photonic and electro-optic devices [59]. The relative permittivity which is also known as optical dielectric constant, exhibit nearly a constant value for PLD-grown ZnO film while for sputtered film its value show sinusoidal variations in the range 1.2 to 1.65 with the wavelength.

The optical conductivity of thin films as a result of the incident photons can be calculated by employing the absorption coefficient and the refractive index using following equation [60]:

$$\sigma = \alpha n \frac{c}{4\pi}. \quad (6)$$

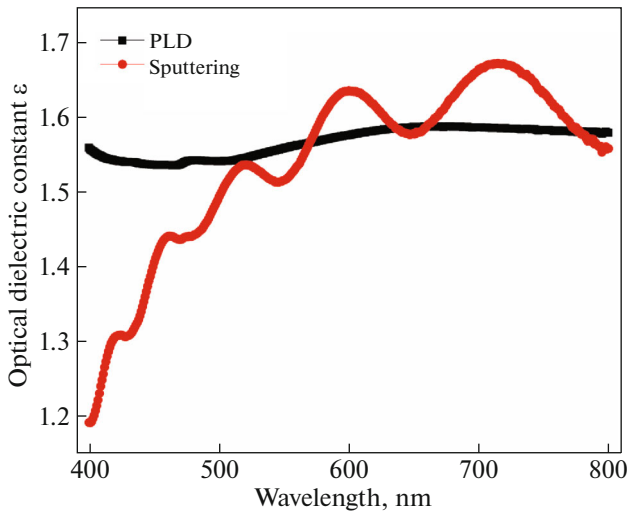


Fig. 10. Curves for optical dielectric constant ϵ versus wavelength.

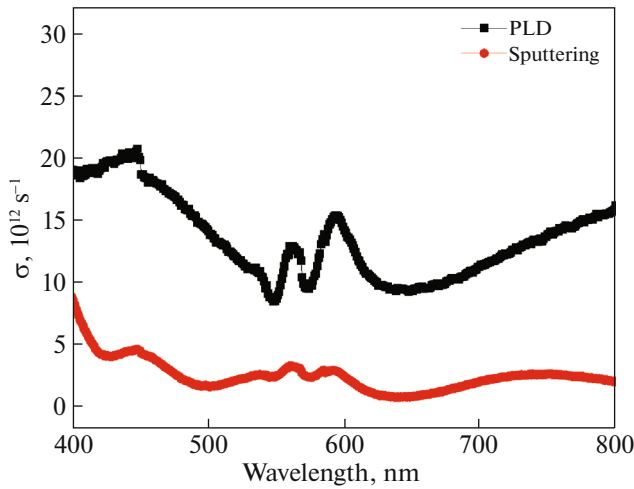


Fig. 11. Plot showing the optical conductivity of ZnO thin films versus wavelength.

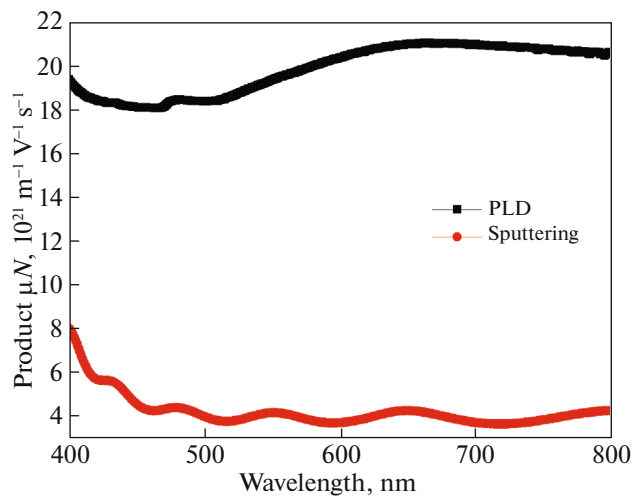


Fig. 12. Plot for the product of carrier concentration and mobility of ZnO thin films versus wavelength.

The range of optical conductivity for sputtering grown ZnO thin film is quite narrow as compared to the PLD-grown ZnO thin film.

The product of carrier concentration N and the carrier mobility μ in the visible wavelength region is shown in Fig. 12 which is found to be dependent on the reflectance R and film thickness x as related by the equation

$$\mu N = 4 \frac{\epsilon_0 c}{[ex(1 - R)]} \tag{7}$$

It can be seen in Fig. 12 that the overall range of product values for PLD sample lies in the higher area as compared to sputtered sample. However, some variations are observed in the product of carrier mobility and carrier concentration for PLD thin film as a function of incident photons wavelength and the product values increase above 550 nm. But for the sputter-deposited sample, the product values found to be quite consistent with the wavelength with no major variation.

Table 1 describes certain room-temperature electrical properties of the PLD-grown and sputtered films.

The carrier concentrations of these films are supplied from donor sites, which are associated with oxygen vacancies and excess metal ions. It is generally believed that the conduction characteristics of ZnO films are dominated by oxygen vacancies and Zn interstitial atoms. The resistivity is inversely proportional to the product of carrier concentration and mobility. Therefore, the change in resistivity with increase in substrate temperature is due to the change in carrier concentration or mobility.

It can be seen that the carrier concentration of ZnO films formed by PLD and sputtering is almost the same. Difference in resistivity is mainly due to the variation of the carrier mobility in each type of film. The columnar growth of ZnO provide high ratio of the grain boundary area as compared to the grains, which in turn provide defective states that are responsible for restriction of the carrier mobility. In PLD sample, the higher crystallinity of the film make us to believe in the formation low-angle grain boundaries among the grains, which in turn decrease the defect density in these regions. On the other hand, the crystallinity of sputtered ZnO film suggests the existence of higher number of defect centers in the grain boundary area among the columnar grains. The grains in sputtered film are combined through high angle boundaries, which increase the grain boundary area to grain ratio and hence higher defect density in that area to effect the mobility of charge carriers. Moreover, the stoichiometry of PLD-grown ZnO films is better than for sputtered films, which also facilitates the higher conductivity of PLD films. Recent investigations suggest that none of demonstrated characteristics are consistent with a high concentration shallow donor. Van de

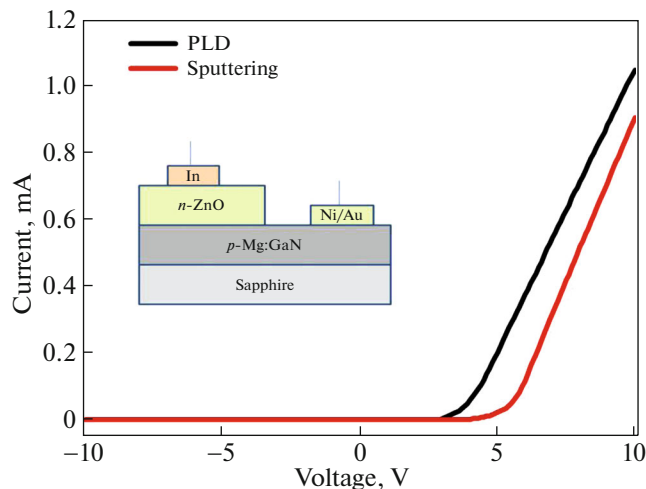
Table 1. Electrical parameters measured by Hall measurement and optical band gap

	Resistivity, $\Omega \text{ cm}$	Mobility, $\text{cm}^2/(\text{V s})$	Carrier concentration, cm^{-3}
PLD	0.0792	34.6	2.28×10^{18}
Sputtering	0.4832	7.5	1.73×10^{18}

Walle [61, 62] gives comprehensive explanation of the native defects and their complexes. He suggests that conductivity is attributed to presence of hydrogen and its complexes with some native defects, which is universal and present during film growth process. Hydrogen impurities react with oxygen vacancies and the resulting complex $(\text{V}_\text{O}\text{H})^\cdot$ behave as a shallow donor in this case, as the PLD-grown films demonstrate better stoichiometry within the grains. But there is a chance for the defects (e.g. oxygen vacancies) present at the grain boundaries to make complexes with $(\text{V}_\text{O}\text{H})^\cdot$. These complexes act as the shallow donors and provide charge carriers for conductivity. Meanwhile, in sputtered sample, the carries provided by these complexes may be scattered or captured by some compensating defects present in the grain boundary area.

The $I(V)$ characteristics of ZnO|GaN junctions are measured by changing the bias voltage from +10 to -10 V. Figure 13 clearly demonstrates the rectifying behavior of the $p-n$ junction diodes.

The forward bias series resistance shown by sputtered sample is larger in comparison to PLD-grown, while reverse bias leakage current for both heterostructures is negligible. The turn-on voltage value of PLD-grown ZnO|GaN junction is 3.8 V while that of

**Fig. 13.** Current–voltage curves of n-ZnO|p-GaN hetero-junction. Inset shows the device structure of hetero-junction.

sputtered-made junction is 5.2 V. The main reasons for the high turn-on voltage in case of sputtered sample include the existence of the interfacial defects and the crystal quality of the ZnO film deposited by the RF magnetron sputtering. As it is evident from the AFM analysis that the surface roughness of sputtered sample is higher than that of PLD sample, so this higher roughness of the film results in accumulation of interfacial defects at the ZnO|GaIn interface. These interfacial defects are responsible for the electron capture when the device is working in the forward bias [63]. The other possible reason is the crystal quality of the ZnO film. As we have seen from the XRD results, the ZnO film made by sputtering has a slightly poorer crystalline structure as compared to PLD.

4. CONCLUSIONS

ZnO films have been grown on the c -plane sapphire substrate by pulsed laser deposition and the RF magnetron sputtering. The sample grown by PLD is showing more crystallinity and smooth surface as compared to the RF-sputtered sample. The higher crystalline quality of PLD-grown film is attributable to energetic flux of incident atoms that provide additional energy to the atoms at the surface. These high energy incident particles have tendency to relieve the internal stresses of the film, which in turn improve the crystallinity of thin film. Phi scan of an oblique angle ZnO (104) plane exhibits the tendency of growth of wurtzite ZnO with six-fold symmetry and higher degree of epitaxial growth in case of PLD-grown sample. More compact columnar growth has been observed in the PLD sample as compared to sputtered one. The columns are separated by large angle boundaries in sputtered sample and give rise to more defects in this region as compared to PLD sample, in which columns are bound by low angle boundaries and possess less number of defects. These defects may be responsible for the reduced electronic mobility in sputtered ZnO film. The blue emissions are observed in the PL spectra of both samples which is attributable to the transition of charge carriers from zinc interstitial to ionized zinc vacancy level. In sputtered sample, the oxygen deficiency has produced strong green emission along with UV and blue luminescence. Both types of defects have expected to be mostly lying in the large angle boundary region of the sputtered sample. The small roughness of PLD-grown ZnO on p-GaIn caused the small number of interfacial defects which results in higher current flow and lower turn-on voltage for the $p-n$ junction diode. This comparison has shown that good crystal quality and low surface roughness are the key factors to be cause for the good electrical behavior of a hetero-junction device, and by controlling these factors we can get a best $p-n$ junction diode for LED applications.

FUNDING

Authors would like to thank Higher Education Commission (HEC), Pakistan for providing financial support of this research.

CONFLICT OF INTEREST

All the authors of this manuscript have no conflict of interest with anyone.

REFERENCES

- M. A. Hernández-Fenollosa, L. C. Damonte, and B. Marí, *Superlatt. Microstruct.* **38**, 336 (2005).
- J. J. Ding, S. Y. Ma, H. X. Chen, X. F. Shi, T. T. Zhou, and L. M. Mao, *Phys. B: Condens. Matter* **404**, 2439 (2009).
- A. Teke, Ü. Özgür, S. Doğan, X. Gu, H. Morkoç, B. Nemeth, J. Nause, and H. Everitt, *Phys. Rev. B* **70**, 195207 (2004).
- P. Zu, Z. K. Tang, G. K. L. Wong, M. Kawasaki, A. Ohtomo, H. Koinuma, and Y. Segawa, *Solid State Commun.* **103**, 459 (1997).
- A. B. Djurišić, W. C. H. Choy, V. A. L. Roy, Y. H. Leung, C. Y. Kwong, K. W. Cheah, T. K. Gundu Rao, W. K. Chan, H. Fei Lui, and C. Surya, *Adv. Funct. Mater.* **14**, 856 (2004).
- R. Hong, H. Qi, J. Huang, H. He, Z. Fan, and J. Shao, *Thin Solid Films* **473**, 58 (2005).
- E. Sonmez, S. Aydin, M. Yilmaz, M. T. Yurtcan, T. Karacali, and M. Ertugrul, *J. Nanomater.* **2012**, 950793 (2012).
- K. Uma, S. Ananthakumar, R. Mangalaraja, T. Soga, and T. Jimbo, *Adv. Mater. Phys. Chem.* **3**, 194 (2013).
- N. Rehman, M. Mehmood, R. Rizwan, M. A. Rasheed, F. C. C. Ling, and M. Younas, *Chem. Phys. Lett.* **609**, 26 (2014).
<https://doi.org/10.1016/j.cplett.2014.05.054>
- X. W. Sun and H. S. Kwok, *J. Appl. Phys.* **86**, 408 (1999).
- D. C. Look, *Mater. Sci. Eng. B* **80**, 383 (2001).
- G. T. Du, W. F. Liu, J. M. Bian, L. Z. Hu, H. W. Liang, X. S. Wang, A. M. Liu, and T. P. Yang, *Appl. Phys. Lett.* **89**, 052113 (2006).
- A. Tsukazaki, A. Ohtomo, T. Onuma, M. Ohtani, T. Makino, M. Sumiya, K. Ohtani, S. F. Chichibu, S. Fuke, Y. Segawa, H. Ohno, H. Koinuma, and M. Kawasaki, *Nat. Mater.* **4**, 42 (2005).
- H. S. Kim, F. Lugo, S. J. Pearton, D. P. Norton, Y.-L. Wang, and F. Ren, *Appl. Phys. Lett.* **92**, 112108 (2008).
- L. G. Wang and A. Zunger, *Phys. Rev. Lett.* **90**, 256401 (2003).
- H.-M. Huang, C.-C. Kuo, C.-Y. Chang, Y.-T. Lin, T.-C. Lu, L.-W. Tu, and W.-F. Hsieh, *J. Electrochem. Soc.* **159**, H290 (2012).
- S. C. Hung, P. J. Huang, C. E. Chan, W. Y. Uen, F. Ren, S. J. Pearton, T. N. Yang, C. C. Chiang, S. M. Lan, and G. C. Chi, *Appl. Surf. Sci.* **255**, 3016 (2008).
- H. Huang, G. Fang, Y. Li, S. Li, X. Mo, H. Long, H. Wang, D. L. Carroll, and X. Zhao, *Appl. Phys. Lett.* **100**, 233502 (2012).
- W. S. Han, Y. Y. Kim, B. H. Kong, and H. K. Cho, *Thin Solid Films* **517**, 5106 (2009).
- X. D. Chen, C. C. Ling, S. Fung, C. D. Beling, Y. F. Mei, R. K. Y. Fu, G. G. Siu, and P. K. Chu, *Appl. Phys. Lett.* **88**, 132104 (2006).
- S. T. Tan, X. W. Sun, J. L. Zhao, S. Iwan, Z. H. Cen, T. P. Chen, J. D. Ye, G. Q. Lo, D. L. Kwong, and K. L. Teo, *Appl. Phys. Lett.* **93**, 013506 (2008).
- J. B. You, X. W. Zhang, S. G. Zhang, H. R. Tan, J. Ying, Z. G. Yin, Q. S. Zhu, and P. K. Chu, *J. Appl. Phys.* **107**, 083701 (2010).
- H. Long, G. Fang, H. Huang, X. Mo, W. Xia, B. Dong, X. Meng, and X. Zhao, *Appl. Phys. Lett.* **95**, 013509 (2009).
- Y. Y. Xi, Y. F. Hsu, A. B. Djurisic, A. M. C. Ng, W. K. Chan, H. L. Tam, and K. W. Cheah, *Appl. Phys. Lett.* **92**, 113505 (2008).
- T. Shu-Yi, H. Min-Hsiung, and L. Yang-Ming, in *Proceedings of the 2011 IEEE International Conference on Nano/Micro Engineered and Molecular Systems NEMS* (2011), p. 1184.
- R. D. Vispute, V. Talyansky, S. Choopun, R. P. Sharma, T. Venkatesan, M. He, X. Tang, J. B. Halpern, M. G. Spencer, Y. X. Li, L. G. Salamanca-Riba, A. A. Iliadis, and K. A. Jones, *Appl. Phys. Lett.* **73**, 348 (1998).
- Y. Nakanishi, A. Miyake, H. Kominami, T. Aoki, Y. Hatanaka, and G. Shimaoka, *Appl. Surf. Sci.* **142**, 233 (1999).
- D. C. Look, D. C. Reynolds, C. W. Litton, R. L. Jones, D. B. Eason, and G. Cantwell, *Appl. Phys. Lett.* **81**, 1830 (2002).
- E. Dalchiele, P. Giorgi, R. Marotti, F. Martín, J. Ramos-Barrado, R. Ayouci, and D. Leinen, *Sol. Energy Mater. Sol. Cells* **70**, 245 (2001).
- Z. Hai, F. Guojia, Z. Yongdan, L. Nishuang, W. Haoning, H. Huihui, L. Songzhan, and Z. Xingzhong, *Eur. Phys. Lett.* **97**, 68001 (2012).
- G.-H. Lee, D.-h. Bae, and W.-J. Lee, *J. Ceram. Process. Res.* **13**, 229 (2012).
- A. Kumar, S. Jeedigunta, I. Tarasov, and S. Ostapenko, *AZO J. Mater. Online* **6**, 1833 (2010).
- W. Zhao-yang, H. Li-zhong, Z. Jie, S. Jie, and W. Zhi-jun, *Vacuum* **78**, 53 (2005).
- A. Aravind, M. K. Jayaraj, M. Kumar, and R. Chandra, *Appl. Surf. Sci.* **286**, 54 (2013).
- H. S. Kim, S. J. Pearton, D. P. Norton, and F. Ren, *Appl. Phys. A* **91**, 255 (2008).
- J. B. You, X. W. Zhang, S. G. Zhang, J. X. Wang, Z. G. Yin, H. R. Tan, W. J. Zhang, P. K. Chu, B. Cui, A. M. Wowchak, A. M. Dabiran, and P. P. Chow, *Appl. Phys. Lett.* **96**, 201102 (2010).
- M. J. C. H. C. Chen, Y. H. Huang, W. C. Sun, W. C. Li, J. R. Yang, H. Kuan, and M. Shiojiri, *IEEE Trans. Electron Dev.* **58** (7), 2122 (2011).
- C.-S. Son, S.-M. Kim, Y.-H. Kim, S.-I. Kim, Y. T. Kim, K. H. Yoon, I.-H. Choi, and H. C. Lopez, *J. Korean Phys. Soc.* **45**, S685 (2004).

39. S. A. M. Lima, F. A. Sigoli, M. Jafelicci, Jr., and M. R. Davolos, *Int. J. Inorg. Mater.* **3**, 749 (2001).
40. V. Nikitenko, in *Zinc Oxide—A Material for Micro- and Optoelectronic Applications*, Ed. by N. Nickel and E. Terukov (Springer, Netherlands, 2005), Vol. 194, p. 69.
41. T. P. Rao and M. C. Santhoshkumar, *Appl. Surf. Sci.* **255**, 4579 (2009).
42. S. Mahmoud, A. H. Eid, and H. Omar, *Fiz. A* **6**, 111 (1997).
43. J.-L. Zhao, X.-M. Li, J.-M. Bian, W.-D. Yu, and X.-D. Gao, *J. Cryst. Growth* **276**, 507 (2005).
44. I. Hamberg and C. G. Granqvist, *J. Appl. Phys.* **60**, R123 (1986).
45. F. K. Shan and Y. S. Yu, *Thin Solid Films* **435**, 174 (2003).
46. B. J. Lokhande and M. D. Uplane, *Appl. Surf. Sci.* **167**, 243 (2000).
47. M. A. Martínez, J. Herrero, and M. T. Gutiérrez, *Sol. Energy Mater. Sol. Cells* **31**, 489 (1994).
48. T. K. Subramanyam, B. Srinivasulu Naidu, and S. Uthanna, *Cryst. Res. Technol.* **8** (34), 981 (1999).
49. Y. Qu, T. A. Gessert, T. J. Coutts, and R. Noufi, *J. Vacuum Sci. Technol. A* **12**, 1507 (1994).
50. P. Beckmann and A. Spizzichino, *The Scattering of Electromagnetic Waves from Rough Surfaces* (Pergamon, Oxford, 1963).
51. A. Ashour, M. A. Kaid, N. Z. El-Sayed, and A. A. Ibrahim, *Appl. Surf. Sci.* **252**, 7844 (2006).
52. N. A. Lange, M. Gordon, and B. S. Forker, *Handbook of Chemistry* (McGraw Hill, New York, 1961).
53. E. M. Bachari, G. Baud, S. Ben Amor, and M. Jacquet, *Thin Solid Films* **348**, 165 (1999).
54. N. Shakti and P. S. Gupta, *Appl. Phys. Res.* **2**, 19 (2010).
55. M. H. Mamat, M. Z. Sahdan, S. Amizam, H. A. Rifaie, Z. Khusaimi, A. Z. Ahmed, S. Abdullah, and M. Rusop, in *Proceedings of the IEEE International Conference on Semiconductor Electronics, ICSE 2008* (2008), p. 566.
56. E. Fortunato, V. Assunção, A. Gonçalves, A. Marques, H. Águas, L. Pereira, I. Ferreira, P. Vilarinho, and R. Martins, *Thin Solid Films* **451–452**, 443 (2004).
57. S. I. Bhat, P. M. Rao, A. P. G. Bhat, and D. K. Avasthi, *Surf. Coat. Technol.* **158–159**, 725 (2002).
58. N. Ponpandian, P. Balaya, and A. Narayanasamy, *J. Phys.: Condens. Matter* **14**, 3221 (2002).
59. W. H. Steier, A. Chen, S.-S. Lee, S. Garner, H. Zhang, V. Chuyanov, L. R. Dalton, F. Wang, A. S. Ren, C. Zhang, G. Todorova, A. Harper, H. R. Fetterman, D. Chen, A. Udupa, D. Bhattacharya, and B. Tsap, *Chem. Phys.* **245**, 487 (1999).
60. P. Sharma and S. C. Katyal, *J. Optoelectron. Adv. Mater.* **9**, 2000 (2007).
61. A. F. Kohan, G. Ceder, D. Morgan, and C. G. van de Walle, *Phys. Rev. B* **61**, 15019 (2000).
62. C. G. van de Walle, *Phys. Rev. Lett.* **85**, 1012 (2000).
63. C.-H. Chen, S.-J. Chang, S.-P. Chang, M.-J. Li, I.-C. Chen, T.-J. Hsueh, and C.-L. Hsu, *Appl. Phys. Lett.* **95**, 223101 (2009).